Synthesis of magnetic recoverable electron-rich TCTA@PVP based conjugated polymer for photocatalytic water remediation and disinfection

Ridha Djellabi[a,b], Jafar Ali[c], Bo Yang[b], Muhammad Rizwan Haider[d], Peidong Su[a,b], Claudia L. Bianchi[e], Xu Zhao[a,*]

[a] *Key Laboratory of Drinking Water Science and Technology, Research Center for Eco-Environmental Sciences, Chinese Academy of Sciences, Beijing, PR China*
[b] *Department of Environmental Engineering, College of Chemistry and Environmental Engineering, Shenzhen University, Shenzhen, PR China*
[c] *Key Laboratory of Environmental Nanotechnology and Health Effects, Research Center for Eco-environmental Sciences, Chinese Academy of Sciences, Beijing, PR China*
[d] *Key Laboratory of Environmental Biotechnology, Research Center for Eco-Environmental Sciences, Chinese Academy of Sciences, Beijing, PR China*
[e] *Department of Chemistry, Università degli Studi di Milano, Via Golgi 19, Milano, Italy*

ABSTRACT

In this study, we report the synthesis of magnetic electron-rich CP@Fe$_3$O$_4$ (Conjugated Polymer (CP) = TCTA-PVP-bipyridine) by hydrothermal method. For this aim, the Fe$_3$O$_4$ nanoparticles were incorporated into photoactive TCTA-PVP-bipyridine based Conjugated Polymer. The photo-redox abilities of CP@Fe$_3$O$_4$ and bare CP were tested for oxidation of methylene blue and reduction of Cr(VI) under UV–visible light and visible light ($\lambda > 420$ nm). The CP@Fe$_3$O$_4$ showed a good ability for performing the Fenton-like reaction by adding H$_2$O$_2$ as oxidizing agent. Additionally, reveals high photocatalytic reduction ability of Cr(VI) for CP@Fe$_3$O$_4$ in compare with bare CP. Furthermore the photocatalytic antibacterial ability of CP@Fe$_3$O$_4$ towards *E. coli* and *Pseudomonas Aerogenosa* in water was studied. The obtained CFU reduction efficiencies were found about 85% and 90% for *E. coli* and *P. Aeruginosa,* respectively. Interestingly the collecting and recyclability of CP@Fe$_3$O$_4$ after photocatalytic reactions were done easily due to its magnetic property.

1. Introduction

The quality of surface and groundwaters influences directly all aspects of humankind.

Industries are most likely the main source of discharged contaminated wastewaters with varying types of toxic compounds including organics, heavy metals and microorganisms. Therefore, water pollution and its treatment has become the most serious concern and a challenging task for the public authorities and industrial world [1]. Due to the huge urbanization and industrialization growth, which is associated with large wastewaters discharged into the environment that overloading the ecosystem, the European Water Framework Directive (WFD) has classified chemical substances into two main categories, namely 'Black List' that includes all highly toxic and non-biodegradable chemicals; and 'Grey List' which involves chemicals that can cause a serious risk to the ecosystem. For clean environment, contaminated industrial wastewaters must be properly treated at the source before discharging them into the environment. The adequate treatment of industrial wastewaters requires usually the combination of different processes because of the complicated nature of such contaminated

waters. The choice of the specific treatment processes mainly depends on several parameters such as the nature and concentration of pollutants in wastewaters, less secondary-waste formation, the simplicity of set-up and cost, the treatment efficiency and so on.

Over more than three decades, heterogeneous photocatalysis for water remediation has traveled an extended path of technological development [2,3]. Photocatalysis system has the competence of continuous oxidizing or reducing a wide range of pollutants in water without producing any toxic secondary waste. Since the efficiency of a photocatalytic treatment system for a targeted contaminated water is directly related to the characteristics of the used photocatalyst, many efforts have been made at a blistering rate aiming to develop novel photoactive materials with better physical and optical characteristics for real-world applications [4,5].

For the sake of enhancing the visible light response (VLR) of photocatalytic materials (i.e., TiO$_2$), band gap engineering was the cornerstone of photocatalytic materials science, therefore, an extensive research has been reported regarding the synthesis of VLR materials through many approaches such as metal and non-metal doping [6–8], dye sensitizing [9,10], semiconductor heterojunction photocatalysts

---

[11,12] and combination of photocatalysts with carbonaceous materials [13,14]. Apart from that, the appropriate use of photocatalyst (supported or suspended in water) for real wastewater treatment has been widely discussed in the literature [15]. Briefly, it was deduced that the dispersed photocatalysts exhibit higher photocatalytic efficiency compared to supported photocatalysts because the immobilized photocatalyst suffers from the low surface area, low irradiated surface and less mass transfer. On contrast, the need of costly post recovery of suspended photocatalyst from water after the treatment is the main issue due to the small sized particles. Therefore, such a trade-off between the high efficiency and the hard recovery of suspended particles must be investigated. For better controllability and easy recovery of the photocatalyst suspension, many studies have been reported on the exploitation of magnetic materials in water remediation [16–19]. Suspended powder-like magnetic photocatalysts can be easily gathered after the treatment via the use of external magnetic field, which indeed facilities the regeneration of the photocatalyst and its reuse. Besides, on top of the magnetic propriety and high stability of Fe_3O_4, it can be also itself photocatalyst to produce reactive oxygen species (ROSs) or electrons under light, or it can catalyze some reactions (i.e., Fenton reaction, Electro-Fenton) [20–23]. On the other hand, some reports mentioned that the introduction of Fe_3O_4 to some semiconductors (i.e., TiO_2) can result in better e^-/h^+ charges separation and VLR [24]. In this study, magnetic Fe_3O_4 was introduced into the electron-rich photoactive TCTA-PVP based conjugated polymer (CP) for better recovery and synergistic photocatalytic effect. The photocatalytic ability of magnetic $CP@Fe_3O_4$ was tested for different types of pollutant that usually exist in wastewaters such as Cr(VI) reduction, methylene blue degradation and for the inactivation of two types of common bacteria in wastewaters (*E. coli* and *Pseudomonas Aeruginosa* (*PA*)) that are known as major faecal contaminant in water purification systems as well [25,26].

2. Experimental section

2.1. Synthesis and characterization of materials

TCTA@PVP based conducting polymer (CP) was synthesized by heat polymerization of Tris(4-carbazoyl-9-ylphenyl)amine (TCTA), PVP and 4, 4′-bipyridine at 70 °C until the color of the mixture changed to orange. The obtained mixture was dried at 90 °C for 48 h and was calcined at 250 °C for 1 h for transformation of the prepared gel to solid blocks.

Fe_3O_4 nanoparticles were synthesized by hydrothermal method [17]. A desired amount of $Fe_3Cl \cdot 6H_2O$ was dissolved in 50 mL of deionizd water, and sonicated for 30 min at room temperature. The mixture was transferred into a sealed, Teflon-lined autoclave and was heated at 180 °C for 6 h. After cooling the mixture to room temperature, the powder was washed several times with distilled water and dried at 60 °C for 12 h.

$CP@Fe_3O_4$ was synthesized via the introduction of Fe_3O_4 particles into the CP orange mixture, and the drying and calcination procedures were continuous. The ratio of $CP:Fe_3O_4$ (g/g) was 8:2.

Materials were characterized by UV–vis Diffuse Reflectance Spectroscopy (UV-DRS), Scanning Electron Microscopy combined with Energy Dispersive Analysis of X-rays (SEM-EDAX), X-ray diffraction (XRD), X-ray Photoelectron Spectroscopy (XPS), Thermogravimetry Differential Scanning Calorimetry (TG-DSC). Cyclic Voltammetry (CV) and Linear Sweep Voltammetry (LSV). TG-DSC was performed on noncalcined photocatalyst samples (the samples after the polymerization were dried at 90 °C for 48 h and then the powder was directly subjected to TG/DSC analysis) using TG/DSC Mettler Toledo from room temperature to 600 °C with a heating rate of 10 °C/min under N_2 atmosphere.

2.2. Photocatalytic experiments

The photocatalytic activities of synthesized materials for degradation of methylene blue dye solution, reduction of hexavalent chromium and inactivation of *Escherichia coli* (*E. coli*) and *Pseudomonas Aeruginosa* (*PA*) in water were studied. PLS-SXE300 Xenon lamp light (PerfectLight) equipped with a quartz UV cut-off filter (λ > 420 nm) was used for the irradiation. The photocatalytic experiments for MB or Cr(VI) removal were carried by mixing 0.25 g/L of the photocatalyst with MB or Cr(VI) solutions under visible light. Aliquots of solution at certain time interval were taken and filtered, and the analysis of Cr(VI) and MB concentrations determined by UV/Vis spectrophotometry at 540 and 662, respectively.

The photocatalytic antibacterial activity of $CP@Fe_3O_4$ composite was evaluated against the *Escherichia coli* and *Pseudomonas aeruginosa*. Purified gram-negative bacterial strains were obtained from the Key Laboratory of Environmental Nanotechnology and Health Effects, CAS, Beijing. The LB broth was used to refresh the culture for further applications in antibacterial tests. The photocatalytic antibacterial activity of $Fe_3O_4@CP$ against both gram negative bacteria was validated through viability of bacterial cells by spread plate method. The spread plate method shows the number of colony forming units (CFU) on plate counter agar. The photocatalytic inactivation of bacteria was evaluated by mixing, in 20 mL test tubes, 20 mg of $CP@Fe_3O_4$ with 15 mL of LB broth and 1 mL of each type of bacteria having 1×10^7 CFU mL^{-1}. LB broth contains 10 gL^{-1} of peptone, 5 gL^{-1} of yeast extract and 10 g/L gL^{-1} of NaCl. Then, test tubes were shacked using Tube Swing Rotary Shaker under PLS-SXE300 Xenon lamp light irradiation (300–1100 nm) at room temperature. Similar test tubes under light without photocatalyst were used as controls. After 2 and 4 h, 200 µL aliquots were aseptically taken out to spread on agar plates. Finally, all the spread agar plates were incubated at 37 °C for 14 h and then the number of bacterial colonies was counted to obtain the CFU reduction efficiency in broth solutions.

3. Results and discussion

3.1. Characterization of materials

In this study, Fe_3O_4 nanoparticles were incorporated into CP platform for synthesis of $CP@Fe_3O_4$ with an enhanced photocatalytic activity and easily separation and recyclability. Fig. 1 shows SEM, EDAX mapping images and EDX spectra of $CP@Fe_3O_4$ composite. According to Fig. 1a, SEM image reveals Fe_3O_4 nanoparticles incorporated. In addition, the agglomeration of Fe_3O_4 nanoparticles on the platform of CP is visible in EDAX mapping images. The EDX spectra of $Fe_3O_4@CP$ composite (Fig. 1g) confirms presence of C, N, O and Fe in its structure and confirms its successful synthesis.

XPS analysis of CP, Fe_3O_4 and $CP@Fe_3O_4$ are shown in Fig. 2. The high-resolution C1s spectrum of bare CP shows three bands at 284.81, 286.52 and 288.42 eV corresponding to $C-C/C=C$, $C-C/C=C-N/$ $C-O$ and $C-C-N/N^+=C-O-$, respectively. C1s spectrum of $CP@Fe_3O_4$ exhibits the same bands as CP spectrum. However, the observed band at 288.42 eV was shifted to 287.31 eV in $CP@Fe_3O_4$ along with an enlargement in the band, which could be due to the contribution of $C-O-Fe$ bonding. The high-resolution O1s spectrum of bare Fe_3O_4 shows a single peak centered at 530.4 eV that is associated to $Fe-O$. While, high-resolution O1s spectrum of $CP@Fe_3O_4$ shows a peak at 531.2 eV resulting from the combination of $Fe-O$ and $Fe-O-C$. The $Fe-O-C$ bonds can be formed as a bridge between CP and Fe_3O_4 [27]. High-resolution N1s spectra of CP and $CP@Fe_3O_4$ show one peak at around 400 eV due to $C-N$ in CP platform bonds $N-C=O$, $N-C=N$ and $N-(C)_3$. High-resolution Fe2p spectrum of Fe_3O_4 exhibits two distinct peaks for $Fe2p_{3/2}$ and $Fe2p_{1/2}$ corresponded to Fe_3O_4 species. However, the incorporation of Fe_3O_4 nanoparticles into FCP was confirmed with EDAX mapping images, the intensities of Fe2p peaks were very weak in
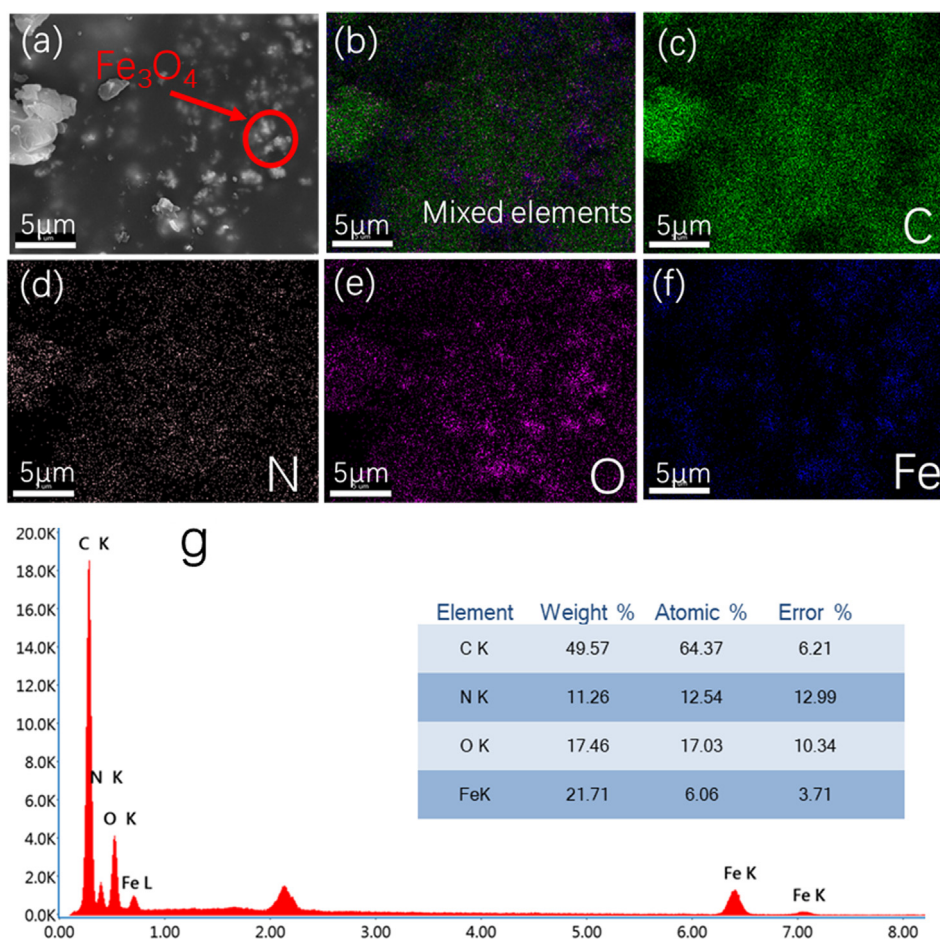
Fig. 1. (a) SEM image of CP@Fe$_3$O$_4$ composite; (b), (c), (d), (e) and (f) are EDAX mapping of mixed elements, C, N, O and Fe, respectively for CP@Fe$_3$O$_4$ composite; (g) EDAX spectrum of CP@Fe$_3$O$_4$ composite.

CP@Fe$_3$O$_4$ which is due to the coverage of most of Fe$_3$O$_4$ particles by CP layer.

The XRD patterns of Fe$_3$O$_4$ and CP@Fe$_3$O$_4$ (Fig. 3a) showcase diffraction peaks corresponded to pure magnetite Fe$_3$O$_4$. Thermogravimetry (TG) and Differential Scanning Calorimetry (DSC) spectra of CP and CP@Fe$_3$O$_4$ are shown in Fig. 3b and c, respectively. TG and DSC analysis (heated from 30 to 600 °C) were performed on non-calcined CP and CP@Fe$_3$O$_4$ samples to check the effect of calcination on the thermal stability of samples. TG curves show two main stages of mass loss. The first one between 80 and 200 °C is attributed to the removal of organic solvent and physically/chemically bounded H$_2$O accompanied by a small mass loss of about 12% and 4% for CP and CP@Fe$_3$O$_4$, respectively. The second stage was occurred in the temperature range of 370 to 440 °C associated with a DSC endothermic peak at around 410 °C which is due to the decomposition of PVP, causing a total mass loss of 91.90 and 57.4% for CP and CP@Fe$_3$O$_4$, respectively.

Fig. 3d and e displays cyclic voltammetry (CV) and linear sweep voltammetry (LSV) of CP and CP@Fe$_3$O$_4$, respectively. It can be seen from the results of CV that the addition of Fe$_3$O$_4$ to CP platform has no effect on the onsets of oxidation and reduction potentials. However, LSV curve of CP@Fe$_3$O$_4$ shows two-step pathway which could be due to the enhanced electrocatalytic activity and better oxygen reduction reaction (ORR) [28]. UV-DRS spectra of photocatalyst samples are shown in Fig. 3f. Clearly, the introduction of Fe$_3$O$_4$ into CP platform results in better visible light response.

The photocatalytic ability of CP@Fe$_3$O$_4$ was tested for the reduction of Cr(VI), oxidation of MB and inactivation of *E. coli* and *PA* in water. For comparison, the photocatalytic efficiency of bare Fe$_3$O$_4$ was evaluated for Cr(VI) reduction under UV–visible and visible light

(> 420 nm) irradiations (Fig. 4a). The adsorption efficiency of bare Fe$_3$O$_4$ towards Cr(VI) solution was found as 8% within 60 min. In terms of Fe$_3$O$_4$/UV–visible and Fe$_3$O$_4$/visible systems, the reduction efficiency towards Cr(VI) solution with initial concentration of 20 mgL^{-1} and pH = 4 was observed as 21% and 12%, respectively. However, the addition of tartaric acid as ROSs and hole scavenger to these two latter systems enhanced the photocatalytic reduction of Cr(VI) species to 80% and 37%, respectively. The results suggest that the Fe$_3$O$_4$ nanoparticles can be photoexcited and produce e$^-$ and h$^+$. The reduction potential of the conduction band of Fe$_3$O$_4$ is not able to reduce O$_2$ to O$_2$$^{\cdot-}$ species, hence two-step reduction occurs for reduction of O$_2$ to H$_2$O$_2$ followed by formation of $\cdot$OH on the conduction band [29]. Direct reduction of Cr(VI) species can happen by photogenerated electrons on the conduction band, meanwhile, the presence of tartaric acid as a scavenger for positive hole and reactive oxygen species (ROSs) results in better electrons generation with longer life. Fig. 4b shows the photocatalytic reduction of Cr(VI) by CP@Fe$_3$O$_4$. According to the results inserted in Fig. 4b, the reduction efficiency of CP@Fe$_3$O$_4$ is much higher than bare Fe$_3$O$_4$ under UV– visible and visible lights which is attributed to the high photoactivity of CP@Fe$_3$O$_4$. Under UV–visible light, 52% of Cr(VI) solution was reduced using CP@Fe$_3$O$_4$ within 60 min, while a total reduction was found at 30 min using CP@Fe$_3$O$_4$/TA. Under visible light, 30% and 65% of Cr(VI) solution within 60 min were reduced by CP@Fe$_3$O$_4$ and CP@Fe$_3$O$_4$/TA systems, respectively.

These reduction reactions are carrying out with the following proposed mechanism. CP can absorb visible light and produces both electrons and ROSs. Unlike Fe$_3$O$_4$, most of ROS (O$_2$$^{\cdot-}$, H$_2O_2$ and $\cdot$OH), which affect the reduction of Cr(VI), can be obtained via single or multi-step reduction of dissolved O$_2$. Furthermore, O$_2$ can compete with
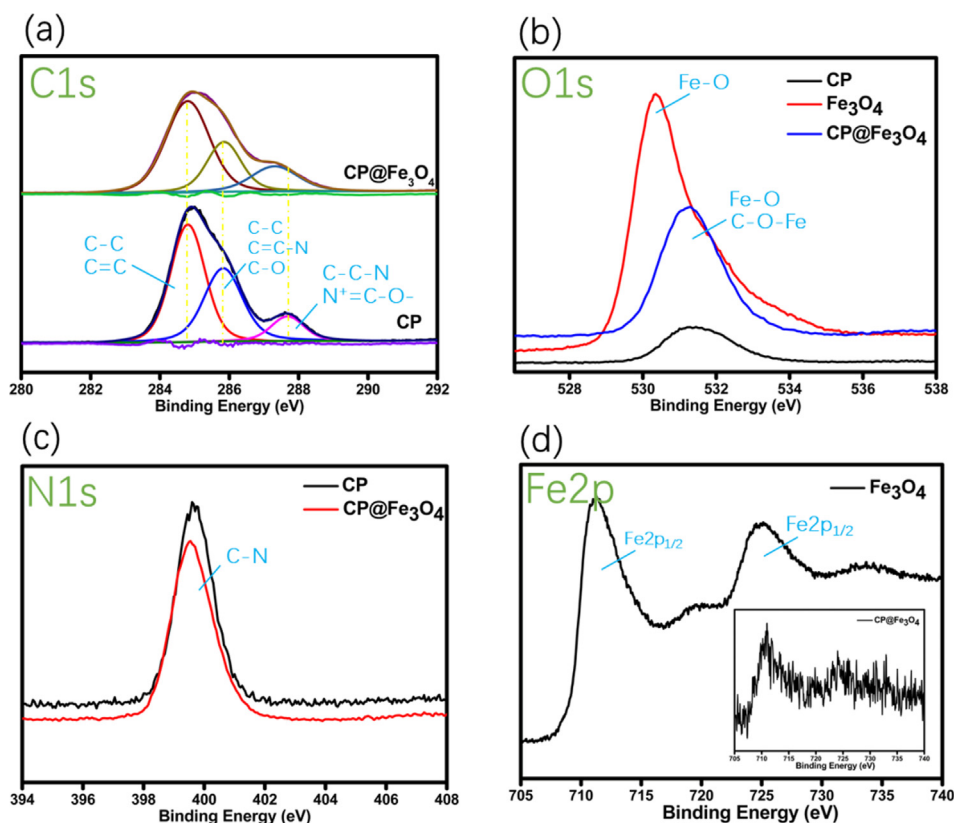
Fig. 2. High-resolution C1s, O1s, N1s and Fe2p spectra of materials.

Cr(VI) species to consume photogenerated electrons on the conduction band of CP.

To investigate this point, an experiment was carried out for reduction of Cr(VI) solution under visible light using CP@Fe$_3$O$_4$ in saturated N$_2$ atmosphere without tartaric acid. As showed in Fig. 4b, a total reduction of Cr(VI) was found within 60 min. This suggests the participation of O$_2$ to consume photogenerated electrons and produce ROSs

which inhibit the reduction of Cr(VI). Additionally, ˙OH can be produced also from h$^+$ of Fe$_3$O$_4$ particles in CP@Fe$_3$O$_4$ composite. The Charges transfer between CP and Fe$_3$O$_4$ is likely to happen, wherein, the transfer of photogenerated electrons from the conduction band of CP platform, which contains electron-rich TCTA with high reduction potential (LUMO level of TCTA is 2.48 V at pH 7), to the conduction band of Fe$_3$O$_4$ is possible, likewise the positive holes can be transferred
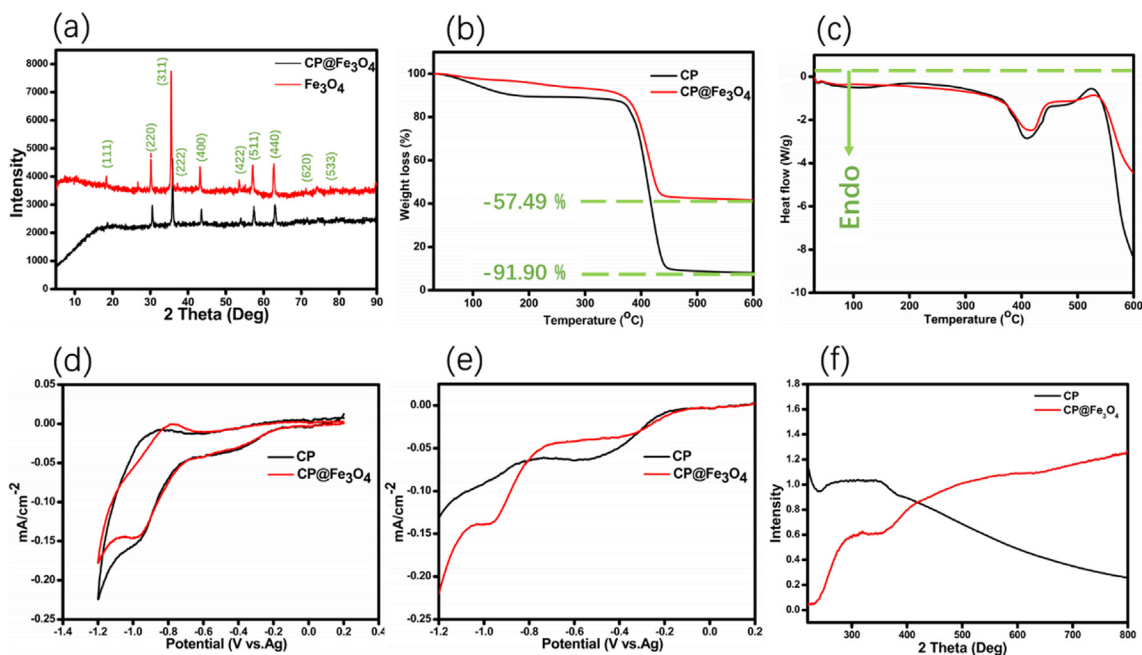

Fig. 3. (a) XRD patterns for Fe$_3$O$_4$ and CP@Fe$_3$O$_4$, (b) TG spectra for CP and CP@Fe$_3$O$_4$, (c) DSC for CP and CP@Fe$_3$O$_4$, (d) CV analysis for CP and CP@Fe$_3$O$_4$, (e) LSV analysis for CP and CP@Fe$_3$O$_4$, and (f) UV-DRS spectra for CP and CP@Fe$_3$O$_4$.
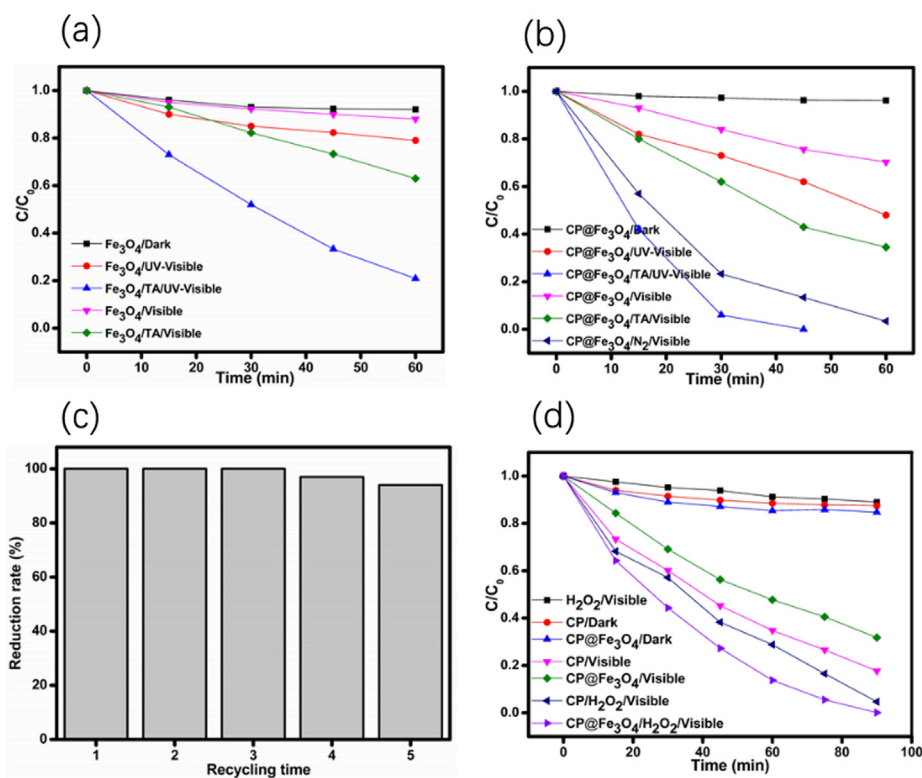
Fig. 4. (a) and (b) Photocatalytic reduction of Cr(VI) with initial concentration of 20 mgL^{-1} using Fe$_3$O$_4$ and CP@Fe$_3$O$_4$ under visible light, respectively, (c) recycling tests of CP@Fe$_3$O$_4$ for Cr(VI) reduction, (d) Photocatalytic oxidation of MB solution with initial concentration of 10 mgL^{-1} using CP and CP@Fe$_3$O$_4$ under visible light irradiation.
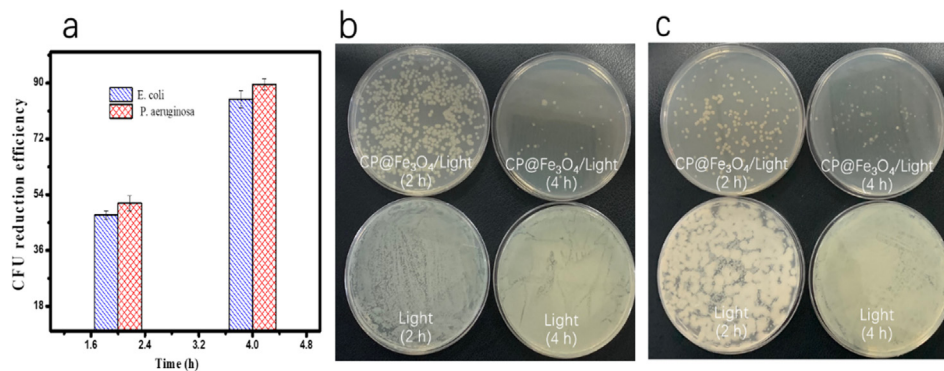

Fig. 5. (a) CFU reduction efficiency of CP@Fe$_3$O$_4$ towards *E. coli* and *PA* under UV–visible light. (b) and (c) images of agar plates after incubation at 37 °C for 14 h for *E. coli* and *PA,* respectively.
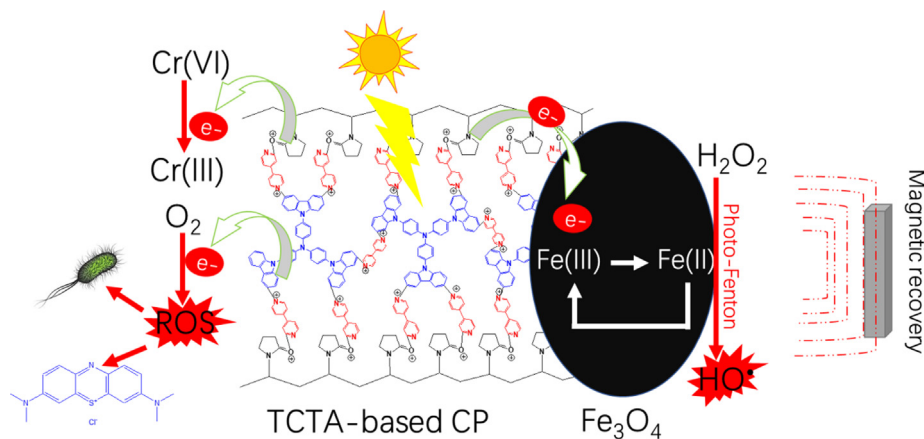

Fig. 6. Mechanism of photocatalytic degradation of organic pollutants, Cr(VI) reduction and bacteria inactivation by CP@Fe$_3$O$_4$. In the presence of H$_2$O$_2$, CP@Fe$_3$O$_4$ can catalyze Fenton reaction.

from the valence band of Fe_3O_4 to CP platform. The electrons of CP transfer to Fe_3O_4 and reduce Fe(III) to Fe(II) species, as a result, the Fe(II) can reduce Cr(VI) directly.

Recycling tests for photocatalytic reduction of Cr(VI) with CP@Fe_3O_4 were performed to check the stability of composite material (Fig. 4c). To avoid the loss of photocatalyst mass during multi-sampling, the concentration of Cr(VI) solution was measured only once after 60 min. The results revealed that after five cycles of reduction process, the reduction efficiency of CP@Fe_3O_4 composite decreases partially.

The photocatalytic oxidation of MB solution under visible light by pure CP and CP@Fe_3O_4 was carried out and the results are showed in Fig. 4d. Obviously, pure CP showed better degradation of MB compared to CP@Fe_3O_4 composite. It seems that pure CP is more active under visible light than CP@Fe_3O_4 to produce ROSs under these conditions. Even with such slight decrease in the efficiency of MB degradation, CP@Fe_3O_4 is more recommended for real-world wastewater remediation because of the easy recovery and recycling. On the contrary, in the presence of 10^{-5} M of H_2O_2, CP@Fe_3O_4 showed better MB oxidation than pure CP. Herein, photo-Fenton reaction catalyzed by Fe_3O_4 may take place for producing more ROSs as shown in Fig. 6. As abovementioned, the transferred electrons from photoexcited CP to Fe_3O_4 resulted in the reduction of Fe(III) to Fe(II) species, which in turn Fe(II) reacts with the added H_2O_2 to generate $\cdot$OH radicals. It is important to point out that Fe_3O_4 itself could contain a little amount of Fe(II) ions on its surface, which can react directly with H_2O_2.

The photocatalytic antibacterial activity of CP@Fe_3O_4 was checked for the inactivation of two types of bacteria i.e., *E. coli* and *Pseudomonas Aeruginosa* (*PA*). Liquid solutions containing *E. coli* or *PA* were subjected to photocatalytic treatment under UV–visible light. Control experiments under UV–visible light without photocatalyst were carried out as well. Afterward, samples after 2 and 4 h were collected and spread on agar plates, and then these agar plates were incubated at 37 °C for 14 h. The results of CFU reduction efficiency are shown in Fig. 5a. CFU reduction efficiency using CP@Fe_3O_4 under UV–visible light was around 85% and 90% for *E. coli* and *PA*, respectively. The results of plate test (Fig. 5b, c) showed a significant inhibition of bacteria in broth solution using CP@Fe_3O_4 under UV–visible, while, intense growth in control plates (without photocatalyst) which further evidences the inhibition of growth was due to generated of ROSs species by CP@Fe_3O_4 under light.

The inactivation of bacteria is occurred by photogenerated ROSs such as $O_2^{\cdot-}$, h^+, $\cdot$OH and H_2O_2. It was reported that ROSs with longer lifetime are more efficient for the inactivation of bacteria, unlike the oxidation of organics [30]. ROSs with longer lifetime are able to damage the bacteria by bursting and collapsing of bacterial membrane and cells. Therefore, H_2O_2 and $O_2^{\cdot-}$, might be more efficient than $\cdot$OH. H_2O_2 can be produced via the reduction of $O_2^{\cdot-}$ by photogenerated electrons in CP@Fe_3O_4 system. Besides the toxic effect of *E. Coli* or *PA*, these species are considered as major faecal contaminants in water purification stations and main contributor for biofouling in membrane systems [26,31].

4. Conclusions

Soft-magnetically recoverable photoactive CP@Fe_3O_4 showed excellent photocatalytic activity for Cr(VI) reduction, MB oxidation and bacteria inactivation. Also, the incorporation of Fe_3O_4 in CP platform facilitates the recovery of the photocatalyst after the water treatment via the application of an external magnetic field. In terms of photoactivity, CP@Fe_3O_4 showed an excellent photocatalytic reduction of Cr(VI) compare to bare CP and Fe_3O_4 under UV–visible and visible light. The incorporation of Fe_3O_4 into CP resulted in lower oxidation of MB compared to bare CP. However the CP@Fe_3O_4 was more efficient in presence of H_2O_2 than bare CP, due to the Fenton reaction achieved by the Fe(II) produced via the reduction of Fe(III) of Fe_3O_4 by

photogenerated electrons coming from CP platform. Interestingly the CP@Fe_3O_4 composite showed very good photocatalytic antibacterial activity against *E. coli* and *Pseudomonas Aeruginosa* in water. Based on the obtained results, CP@Fe_3O_4 composite, can be used as an efficient photocatalyst for water remediation and disinfection in wastewater treatment.

Declaration of Competing Interest

The authors declare that they have no known competing financial interests or personal relationships that could have appeared to influence the work reported in this paper.

Acknowledgements

Appendix A. Supplementary material

Supplementary data to this article can be found online at https://doi.org/10.1016/j.seppur.2020.116954.

References

[1] G. Crini, E. Lichtfouse, Advantages and disadvantages of techniques used for wastewater treatment, Environ. Chem. Lett. 17 (2019) 145–155.

[2] S. Dong, J. Feng, M. Fan, Y. Pi, L. Hu, X. Han, M. Liu, J. Sun, J. Sun, Recent developments in heterogeneous photocatalytic water treatment using visible light-responsive photocatalysts: a review, RSC Adv. 5 (2015) 14610–14630.

[3] M.N. Chong, B. Jin, C.W. Chow, C. Saint, Recent developments in photocatalytic water treatment technology: a review, Water Res. 44 (2010) 2997–3027.

[4] S. Sun, X. Yu, Q. Yang, Z. Yang, S. Liang, Mesocrystals for photocatalysis: a comprehensive review on synthesis engineering and functional modifications, Nanoscale Adv. 1 (2019) 34–63.

[5] Fen Zhang, Yongcai Zhang, Geshan Zhang, Zhanjun Yang, Dionysios D. Dionysiou, Aiping Zhu, Exceptional synergistic enhancement of the photocatalytic activity of SnS_2 by coupling with polyaniline and N-doped reduced graphene oxide, Appl. Catal. B. 236 (2018) 53–63.

[6] L.G. Devi, R. Kavitha, A review on non metal ion doped titania for the photocatalytic degradation of organic pollutants under UV/solar light: role of photogenerated charge carrier dynamics in enhancing the activity, Appl. Catal. B Environ. 140 (2013) 559–587.

[7] M. Nolan, Surface modification of TiO_2 with metal oxide nanoclusters: a route to composite photocatalytic materials, Chem. Commun. 47 (2011) 8617–8619.

[8] J.H. Shah, M. Fiaz, M. Athar, J. Ali, M. Rubab, R. Mehmood, S.U.U. Jamil, R. Djellabi, Facile synthesis of N/B-double-doped Mn_2O_3 and WO_3 nanoparticles for dye degradation under visible light, Environ. Technol. 1–10 (2019).

[9] X. Zhang, T. Peng, S. Song, Recent advances in dye-sensitized semiconductor systems for photocatalytic hydrogen production, J. Mater. Chem. A 4 (2016) 2365–2402.

[10] Z. Youssef, P. Arnoux, L. Colombeau, J. Toufaily, T. Hamieh, C. Frochot, T. Roques-Carmes, Comparison of two procedures for the design of dye-sensitized nanoparticles targeting photocatalytic water purification under solar and visible light, J. Photochem. Photobiol., A. 356 (2018) 177–192.

[11] Z. Zhang, W. Wang, L. Wang, S. Sun, Enhancement of visible-light photocatalysis by coupling with narrow-band-gap semiconductor: a case study on Bi_2S_3/Bi_2WO_6, ACS Appl. Mater. Interfaces 4 (2012) 593–597.

[12] H. Wang, L. Zhang, Z. Chen, J. Hu, S. Li, Z. Wang, J. Liu, X. Wang, Semiconductor heterojunction photocatalysts: design, construction, and photocatalytic performances, Chem. Soc. Rev. 43 (2014) 5234–5244.

[13] R. Djellabi, B. Yang, K. Xiao, Y. Gong, D. Cao, H.M.A. Sharif, X. Zhao, C. Zhu, J. Zhang, Unravelling the mechanistic role of Ti-OC bonding bridge at titania/lignocellulosic biomass interface for Cr (VI) photoreduction under visible light, J. Colloid Interface Sci. 553 (2019) 409–417.

[14] J. Ge, Y. Zhang, S.-J. Park, Recent advances in carbonaceous photocatalysts with enhanced photocatalytic performances: a mini review, Materials 12 (2019) 1916.

[15] A.Y. Shan, T.I.M. Ghazi, S.A. Rashid, Immobilisation of titanium dioxide onto supporting materials in heterogeneous photocatalysis: a review, Appl. Catal., A. 389 (2010) 1–8.

[16] R. Du, Q. Zhao, Z. Zheng, W. Hu, J. Zhang, 3D self-supporting porous magnetic assemblies for water remediation and beyond, Adv. Energy Mater. 6 (2016) 1600473.

[17] R. Djellabi, B. Yang, H.M.A. Sharif, J. Zhang, J. Ali, X. Zhao, Sustainable and easy recoverable magnetic TiO_2-lignocellulosic biomass@ Fe_3O_4 for solar photocatalytic

water remediation, J. Clean. Prod. 233 (2019) 841–847.

[18] H.M.A. Sharif, A. Mahmood, H.-Y. Cheng, R. Djellabi, J. Ali, W.-L. Jiang, S.-S. Wang, M.R. Haider, N. Mahmood, A.-J. Wang, Fe_3O_4 nanoparticles coated with EDTA and Ag nanoparticles for the catalytic reduction of organic dyes from wastewater, ACS Appl Nano Mater. 2 (2019) 5310–5319.

[19] R.D. Ambashta, M. Sillanpää, Water purification using magnetic assistance: a review, J. Hazard. Mater. 180 (2010) 38–49.

[20] P. Mishra, S. Patnaik, K. Parida, An overview of recent progress on noble metal modified magnetic Fe_3O_4 for photocatalytic pollutant degradation and H_2 evolution, Catal. Sci 9 (2019) 916–941.

[21] W. Wang, Q. Mao, H. He, M. Zhou, Fe_3O_4 nanoparticles as an efficient heterogeneous Fenton catalyst for phenol removal at relatively wide pH values, Water Sci. Technol. 68 (2013) 2367–2373.

[22] Z. He, C. Gao, M. Qian, Y. Shi, J. Chen, S. Song, Electro-Fenton process catalyzed by Fe_3O_4 magnetic nanoparticles for degradation of CI Reactive Blue 19 in aqueous solution: operating conditions, influence, and mechanism, Ind. Eng. Chem. Res. 53 (2014) 3435–3447.

[23] S.-T. Yang, W. Zhang, J. Xie, R. Liao, X. Zhang, B. Yu, R. Wu, X. Liu, H. Li, Z. Guo, $Fe_3O_4@SiO_2$ nanoparticles as a high-performance Fenton-like catalyst in a neutral environment, RSC Adv. 5 (2015) 5458–5463.

[24] B. Mercyrani, R. Hernandez-Maya, M. Solís-López, C. Th-Th, S. Velumani, Photocatalytic degradation of Orange G using TiO_2/Fe_3O_4 nanocomposites, J. Mater. Sci-Mater. El. 29 (2018) 15436–15444.

[25] J. Ali, L. Wang, H. Waseem, H.M.A. Sharif, R. Djellabi, C. Zhang, G. Pan,

[26] S. Rana, U. Nazar, J. Ali, Q.U.A. Ali, N.M. Ahmad, F. Sarwar, H. Waseem, S.U.U. Jamil, Improved antifouling potential of polyether sulfone polymeric membrane containing silver nanoparticles: self-cleaning membranes, Environ. Technol. 39 (2018) 1413–1421.

[27] J. Lin, H. Liang, H. Jia, S. Chen, J. Guo, J. Qi, C. Qu, J. Cao, W. Fei, J. Feng, In situ encapsulated Fe_3O_4 nanosheet arrays with graphene layers as an anode for high-performance asymmetric supercapacitors, J. Mater. Chem. A 5 (2017) 24594–24601.

[28] S. Wang, D. Yu, L. Dai, Polyelectrolyte functionalized carbon nanotubes as efficient metal-free electrocatalysts for oxygen reduction, J. Am. Chem. Soc. 133 (2011) 5182–5185.

[29] U. Kurien, Z. Hu, H. Lee, A.P. Dastoor, P.A. Ariya, Radiation enhanced uptake of Hg 0 (g) on iron (oxyhydr) oxide nanoparticles, RSC Adv. 7 (2017) 45010–45021.

[30] W. Wang, L. Zhang, T. An, G. Li, H.-Y. Yip, P.-K. Wong, Comparative study of visible-light-driven photocatalytic mechanisms of dye decolorization and bacterial disinfection by B-Ni-codoped TiO_2 microspheres: The role of different reactive species, Appl. Catal. B Environ. 108 (2011) 108–116.

[31] K. Khan, Y. Lu, M.A. Saeed, H. Bilal, H. Sher, H. Khan, J. Ali, P. Wang, H. Uwizeyimana, Y. Baninla, Prevalent fecal contamination in drinking water resources and potential health risks in Swat, Pakistan, J. Environ. Sci. 72 (2018) 1–12.

Bioelectrochemical recovery of silver from wastewater with sustainable power generation and its reuse for biofouling mitigation, J. Clean. Prod. 235 (2019) 1425–1437.